*32nd EPS Conference on Plasma Phys. Tarragona, 27 June - 1 July 2005 ECA Vol.**29C**, P-4.013 (2005)*

Compatibility of the Radiating Divertor With High Performance Plasmas in DIII-D

T.W. Petrie[1], M.R. Wade[1], S.L. Allen[2], N.H. Brooks[1], M.E. Fenstermacher[2], J.R. Ferron[1], C.M. Greenfield[1], M. Groth[2], A.W. Hyatt[1], C.J. Lasnier[2], A.W. Leonard[1], T.C. Luce[1], M.A. Mahdavi[1], M.J. Schaffer[1], J.G. Watkins[3], W.P. West[1], and the DIII–D Team

[1]*General Atomics, P.O. Box 85608, San Diego, California 92186-5608, USA*
[2]*Lawrence Livermore National Laboratory, Livermore, California, USA*
[3]*Sandia National Laboratories, Albuquerque, New Mexico, USA*

Excessive thermal power loading on the divertor structures presents a design difficulty for future-generation, high powered tokamaks. This difficulty may be mitigated by "seeding" the divertor with impurities which radiate a significant fraction of the power upstream of the divertor targets. For this "radiating divertor" concept to be practical, however, the confinement and stability of the plasma cannot be compromised by excessive leakage of the seeded impurities into the core plasma. One proposed way of reducing impurity influx is to enhance the directed scrape-off layer (SOL) flow of deuterium ions toward the divertor [1-5].

We report here on the successful application of the radiating divertor scenario to high performance plasma operation in a DIII-D "hybrid" H-mode regime. The "hybrid" regime [6,7] has many features in common with conventional ELMing H-mode regimes, such as high confinement, e.g., $H_{ITER89P} > 2$, where $H_{ITER89P}$ is the energy confinement normalized to the 1989 ITER L-mode scaling [8]. The main difference is the absence of sawtooth activity in the hybrid. Argon was selected as the seeded impurity for this experiment because argon radiates effectively at both the divertor and pedestal temperatures found in DIII-D hybrid H-mode operation and has a relatively short ionization mean free path. Carbon is also present as the dominant intrinsic impurity in DIII-D discharges.

The geometry of this experiment is shown in Fig. 1. A double-null cross-sectional shape was biased upward (dRsep = +1.0 cm). To increase the deuterium ion flow toward the divertor at the top of the vessel, deuterium gas was introduced near the bottom. Argon was injected directly into the private flux region (PFR) of the upper divertor. In-vessel pumping of deuterium and argon was done by cryopumps located in the two upper divertor plenums, shown in cross-hatching [9]. The upper divertor, which we hereafter will simply refer to as the "divertor", is the region lying above the dashed line in Fig. 1, and is relatively "closed."

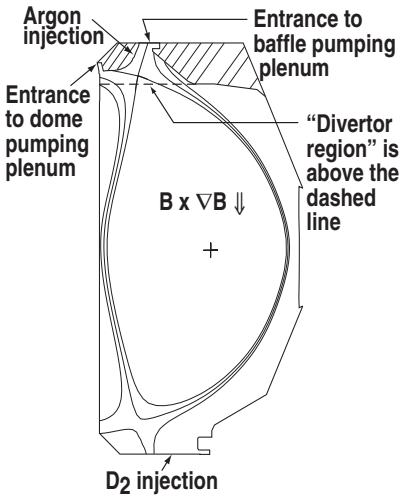

Fig. 1. Particle pumping- and gas injection locations are superimposed on the plasma cross-section. The "divertor region" lies above the dashed line.

The global parameters in this experiment were: plasma current I_p = 1.2 MA, toroidal field B_T = 1.8 T with the $\boldsymbol{B}\times\nabla\boldsymbol{B}$ ion drift directed downward, q_{95} = 4.3,

power input P_{IN} = (5–7) MW, line-averaged density $n_{e,ave}$ = (0.4–0.7)x10^{20} m^{-3} (or $n_{e,ave}/n_G$ = 0.40-0.65, where n_G is the Greenwald density [10]), and $H_{ITER,89P}$ = 2.0-2.5. These discharges, operating in the Type-1 ELMing regime, had stationary-state phases lasting >3 s.

A measure of how well the injected argon is preferentially confined to the divertor is the *exhaust enrichment*: $\eta_{EXH} \equiv f_{EXH}/f_{core}$, where f_{EXH} is the ratio of the neutral argon pressure in the baffle plenum to the atomic-equivalent pressure of deuterium, and f_{core} is the ratio of impurity density to electron density. Absolute measurements of the spatial profiles of He-like argon and fully-stripped carbon in the core plasma were made using charge-exchange recombination spectroscopy [11]. A Penning gauge made simultaneous measurement of the partial pressures of argon and deuterium in the exhaust gas [12].

For *trace* argon injection, the argon concentration $f_{AR,core}$ ($\equiv n_{AR}/n_e$ at radial location ρ = 0.7) was determined for three deuterium injection rates Γ_{D2} (Table 1). We chose ρ = 0.7, because the MIST [13] impurity transport analysis of these plasmas indicated that helium-like argon at $\rho \approx 0.7$ was by far the dominant charge state of argon and was thus a good approximation for the total argon density; ρ = 0.7 is located 10 cm inboard of the outer midplane separatrix. When Γ_{D2} was increased, $f_{AR,core}$ decreased while η_{EXH} rose proportionately with Γ_{D2}. The ELM frequency (ν_{ELM}) also increased with Γ_{D2}.

Table 2 summarizes the response of the hybrid plasmas to changes in the argon injection rate (Γ_{AR}) at radiatively significant levels; Γ_{D2} was the same for the three cases. When the "high" Γ_{AR} (Case 3) is compared with the trace Γ_{AR} (Case 1), we find for the high Γ_{AR} case that: (1) The total radiated power fraction $P_{Rad,tot}/P_{IN}$ increased from 0.46 to 0.62, and both core radiation $P_{Rad,core}$ and divertor radiation $P_{Rad,div}$ increased by about the same amount, (2) The normalized peak heat flux at the outer diverter target $Q_{peak}/Q_{peak,1}$ fell by ≈40%, where the peak heat flux has been normalized to Case 1, and (5) The Type-I ELM (frequency (ν_{ELM}) was unchanged at ≈70 Hz. Electron temperature at the outer divertor target decreased from ≈15 eV (Case 1) to ≈9 eV (Case 3), and both inner and outer divertor legs were "attached" during argon injection in all three cases.

While the core carbon concentration n_C/n_e was almost unchanged for Cases 1-3, the absolute amount of carbon was slightly higher in Case 3 than in Case 1. An increase

Table 1. Trace argon injection at three levels of deuterium injection

	Case A	Case B	Case C
Γ_{D2} (particles/s × 10^{21})	0	3.4	7.1
Γ_{AR} (particles/s × 10^{19})	1.3	1.3	1.3
n_{AR}/n_e (ρ=0.7) (%)	0.092	0.034	0.013
η_{EXH}	11.4	24.3	35.1
$n_{e,ave}$ (10^{20} m^{-3})	0.47	0.58	0.61
ν_{ELM}	40	55	70

Table 2. Three levels of argon injection at fixed deuterium injection

Note: $\beta_N \approx 2.4$ in All Cases	D_2 + Argon (Case 1)	D_2 + Argon (Case 2)	D_2 + Argon (Case 3]
Γ_{D2} (particles/s x 10^{21})	7.1	7.1	7.1
Γ_{AR} (particles/s x 10^{19})	1.3	11.3	21.3
$n_{e,ave}$ (10^{20} m^{-3})	0.61	0.64	0.67
$H_{ITER\ 89P}$	1.9	2.0	2.0
P_{IN} (MW)	6.9	6.8	6.6
$P_{Rad,tot}/P_{IN}$	0.46	0.53	0.62
$P_{Rad,cor}/P_{IN}$	0.17	0.20	0.24
$P_{Rad,div}/P_{IN}$	0.15	0.18	0.21
$Q_{Peak}/Q_{Peak,1}$	1.0	-	0.58
ν_{ELM} (Hz)	≈70	≈70	≈70
n_e (ρ = 0.7) (10^{20} m^{-3})	0.52	0.53	0.55
n_C/n_e (ρ= 0.7) (%)	2.9	3.1	3.0
n_{AR}/n_e (ρ= 0.7) (%)	0.013	0.10	0.19
Z_{eff} [ρ = 0.7]	1.9	2.2	2.4
η_{EXH}	35.1	35.1	34.4

in Γ_{AR} led to a pronounced increase in both n_{AR}/n_e and core Z_{eff}, the latter almost entirely due to the additional argon in the core. Γ_{AR} for Case 3 was about 16 times that of Case 1, and n_{AR} for Case 3 was also about 16 times that of Case 1. Hence, for $\Gamma_{AR} \leq 2.1 \times 10^{20}$ particles/s, $n_{AR} \propto \Gamma_{AR}$, while η_{EXH} was insensitive to Γ_{AR}. This contrasts with a previous study done in a more open DIII-D divertor, where η_{EXH} decreased markedly at higher levels of Γ_{AR} [4].

The radiated power profiles for the three cases in Table 2 are shown in Fig. 2. With only a trace amount of argon in the core, the radiated power profile was predominantly due to carbon. Using measured n_e, T_e, n_{AR}, and radiated power plus the radiation emission rates for argon [14], we estimate that more than 70% of the *increase* in radiated power between trace and high Γ_{AR} cases was due to argon. Yet, the primary radiator inside the core plasma remained carbon in all cases. For even the high Γ_{AR} case, the fraction of the radiated power due to argon was only about one-quarter of the total radiated power from the core.

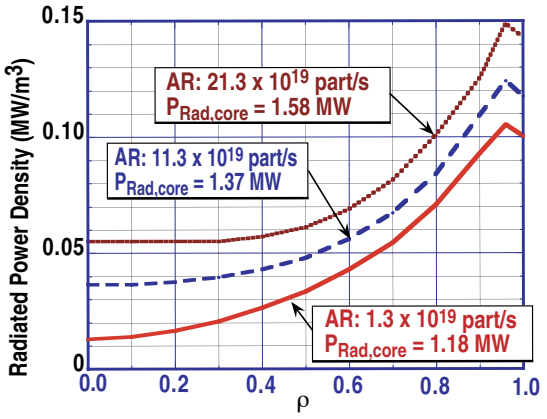

Fig. 2. The radiated power densities for the three D_2 + argon injection cases are plotted as a function of normalized radial coordinate ρ.

Approximately 40% of the increase in $P_{Rad,tot}$ between the trace and high Γ_{AR} cases was in the core and another ≈40% was in the divertor. The other 20% was in the SOL. Figures 3(a,b) show similarities in the distribution of divertor radiated power for both cases. There were three localized regions of peaked emissivity: along the inboard divertor leg, along the outboard baffle, and near the outer divertor target. The main difference in the radiation distribution in the divertor was that the peak emissivity near the outer divertor target was ≈2.5x higher for the high Γ_{AR} case than for the trace case.

Separate measurements of the radiated power due to argon, carbon, and deuterium were not available for the divertor. Still inferences from available spectroscopic and bolometric data can be drawn. Since little argon was present in Case 1, $P_{Rad,div}$ would have to be from carbon and/or deuterium. Since both divertor legs were attached and $T_e \approx 15$ eV at the divertor targets, the peaks in deuterium emissivity would be localized at or near the inner and outer divertor targets, and this was confirmed by the camera monitoring D_α (656.3 nm) radiation in the divertor. The CIII (465 nm) radiation in the divertor was monitored by a second camera. Divertor spectroscopy has shown previously that CIII emission is a good indicator of the location of the dominant radiator CIV lines. In contrast with deuterium, the CIII inversions display distribution much more consistent with the bolometric inversions. We thus infer that $P_{Rad,div}$ was predominantly from carbon.

We also infer that carbon must be the main radiator in the divertor at high Γ_{AR}. The CIII inversions for trace and high Γ_{AR} cases are similar, suggesting no major change in the carbon radiated power. The CII (514.7 nm) inversions, representing a kind of "carbon source" distri-

bution in the divertor, shows little change across most of the divertor, except for a 50% increase in the CII signal at the outer divertor target in the high Γ_{AR} case. At the outer divertor target, both the ARII (433.1 nm) signal and the CII signal are proportional to Γ_{AR}, suggesting the possibility of carbon sputtering by argon, which could be facilitated by the combination of a large thermal deuterium flux at the target with the impinging argon ions [15]. Assuming the entire increase in divertor radiation between trace and high Γ_{AR} cases were due to argon, an upper bound on the ratio of the argon contribution to the total divertor radiation in the high Γ_{AR} case is ≈0.29, which would be about twice the *measured* value reported in [4].

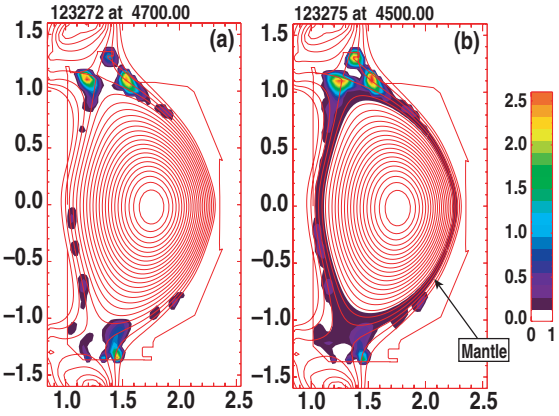

Fig. 3. Tomographic inversions of bolometer data show the poloidal distribution of the radiated power density for (a) Case 1 and (b) Case 3.

This experiment was the first attempt at melding a radiating divertor scenario with a high performance hybrid plasma. Argon puffing into the PFR in combination with D_2 injection into the SOL was effective in reducing power loading at the divertor targets by raising $P_{Rad,core}$ and $P_{Rad,div}$ in near proportionality to Γ_{AR} over the range in Γ_{AR} studied. The insensitivity of η_{EXH} to Γ_{AR} at fixed Γ_{D2} suggests that the plasma could have tolerated even higher levels Γ_{AR} while still maintaining acceptable hybrid performance. Moreover, the linear response of $P_{Rad,core}$ and $P_{Rad,div}$ to Γ_{AR} suggests that feedback control of Γ_{AR} to maximize the radiated power should be possible, as proposed earlier in [4].

A clear tradeoff exists between desirable reduction in heat flux from enhanced radiated power and unfavorable fuel ion displacement in the core plasma by the argon. Argon accumulation in the core may be ameliorated by increasing Γ_{D2}. We also note that, even in the high Γ_{AR} case and *without* sawteeth present, the radiated power profile is not peaked on axis. Whether or not this means that the hybrid plasma can "naturally" resist the accumulation of impurities on axis without sawteeth will be the subject of future investigation.

This work was supported by the U.S. Department of Energy under DE-FC02-04ER54698, W-7405-ENG-48, and DE-AC04-94AL85000.

[1] M.J. Schaffer, *et al*., Nucl. Fusion **35** (1995) 1000.
[2] M.J. Schaffer, *et al*., J. Nucl. Mater. **241-243** (1997) 585.
[3] M.R. Wade, *et al*., Nucl. Fusion **38** (1998) 1839.
[4] M.R. Wade, *et al*., J. Nucl. Mater. **266-269** (1999) 44.
[5] J.A. Goetz, *et al*., J. Nucl. Mater. **266-269** (1999) 359.
[6] T.C. Luce, *et al*., Nucl. Fusion **43** (2003) 321.
[7] M.R. Wade, *et al*., Proc. 20th IAEA Fusion Energy Conf., Vilamoura, Portugal, 2004.
[8] P.N. Yushmanov, *et al*., Nucl. Fusion **30** (1990) 1999.
[9] T.W. Petrie, *et al*., J. Nucl. Mater. **337-339** (2005) 216.
[10] M. Greenwald, *et al*., Nucl. Fusion **28** (1988) 2199.
[11] P. Gohil, *et al*., Proc. of the 14th IEEE/NPSS Symposium on Fusion Engineering, San Diego, 1991.
[12] C.C. Klepper, D.L. Hillis, M.R. Wade, *et al*., Rev. Sci. Instrum. **68** (1997) 400.
[13] R.A. Hulse, Nucl. Technol. Fusion **3** (1983) 259.
[14] R. Clark, J. Abdallah, D.E. Post, J. Nucl. Mater. **220-222** (1995) 1028.
[15] C. Hopf, A. von Keudell, and W. Jacob, Nucl. Fusion **42** (2003) L27.